Research Article | Vol. 26, No. 18 | 3 Sep 2018 | OPTICS EXPRESS 22801
Optics EXPRESS

Design of a tapered slot waveguide dielectric laser accelerator for sub-relativistic electrons

ZHEXIN ZHAO,[1] TYLER W. HUGHES,[2] SI TAN,[2] HUIYANG DENG,[1] NEIL SAPRA,[3] R. JOEL ENGLAND,[4] JELENA VUCKOVIC,[1] JAMES S. HARRIS,[1] ROBERT L. BYER,[2] AND SHANHUI FAN[1,*]

[1]*Department of Electrical Engineering, 350 Serra Mall, Stanford University, CA 94305, USA*
[2]*Department of Applied Physics, 348 Via Pueblo, Stanford University, CA 94305, USA*
[3]*Department of Physics, 382 Via Pueblo Mall, Stanford University, CA 94305, USA*
[4]*SLAC National Accelerator Laboratory, 2575 Sand Hill Rd, Menlo Park, CA 94025, USA*
[*]*shanhui@stanford.edu*

Abstract: We propose a dielectric laser accelerator design based on a tapered slot waveguide structure for sub-relativistic electron acceleration. This tapering scheme allows for straightforward tuning of the phase velocity of the accelerating field along the propagation direction, which is necessary for maintaining synchronization with electrons as their velocities increase. Furthermore, the non-resonant nature of this design allows for better tolerance to experimental errors. We also introduce a method to design this continuously tapered structure based on the eikonal approximation, and give a working example based on realistic experimental parameters.

OCIS codes: (230.7370) Waveguides; (320.0320) Ultrafast optics; (230.0230) Optical devices.

References and links

1. G. Adamo, K. F. MacDonald, Y. Fu, C. Wang, D. Tsai, F. G. de Abajo, and N. Zheludev, "Light well: a tunable free-electron light source on a chip," Physical Review Letters **103**, 113901 (2009).
2. L. J. Wong, I. Kaminer, O. Ilic, J. D. Joannopoulos, and M. Soljačić, "Towards graphene plasmon-based free-electron infrared to x-ray sources," Nature Photonics **10**, 46 (2016).
3. F. Liu, L. Xiao, Y. Ye, M. Wang, K. Cui, X. Feng, W. Zhang, and Y. Huang, "Integrated cherenkov radiation emitter eliminating the electron velocity threshold," Nature Photonics **11**, 289–292 (2017).
4. E. Peralta, K. Soong, R. England, E. Colby, Z. Wu, B. Montazeri, C. McGuinness, J. McNeur, K. Leedle, D. Walz, E. Sozer, B. Cowan, B. Schwartz, G. Travish, and R. Byer, "Demonstration of electron acceleration in a laser-driven dielectric microstructure," Nature **503**, 91–94 (2013).
5. T. Plettner, P. Lu, and R. Byer, "Proposed few-optical cycle laser-driven particle accelerator structure," Physical Review Special Topics-Accelerators and Beams **9**, 111301 (2006).
6. J. Breuer and P. Hommelhoff, "Laser-based acceleration of nonrelativistic electrons at a dielectric structure," Physical Review Letters **111**, 134803 (2013).
7. K. Soong, R. Byer, E. Colby, R. England, and E. Peralta, "Laser damage threshold measurements of optical materials for direct laser accelerators," AIP Conference Proceedings **1507**, 511–515 (2012).
8. S. T. Cundiff and J. Ye, "Colloquium: Femtosecond optical frequency combs," Reviews of Modern Physics **75**, 325 (2003).
9. K. P. Wootton, Z. Wu, B. M. Cowan, A. Hanuka, I. V. Makasyuk, E. A. Peralta, K. Soong, R. L. Byer, and R. J. England, "Demonstration of acceleration of relativistic electrons at a dielectric microstructure using femtosecond laser pulses," Optics Letters **41**, 2696–2699 (2016).
10. R. J. England, R. J. Noble, K. Bane, D. H. Dowell, C.-K. Ng, J. E. Spencer, S. Tantawi, Z. Wu, R. L. Byer, E. Peralta, K. Soong, C.-M. Chang, B. Montazeri, S. J. Wolf, B. Cowan, J. Dawson, W. Gai, P. Hommelhoff, Y.-C. Huang, C. Jing, C. McGuinness, R. B. Palmer, B. Naranjo, J. Rosenzweig, G. Travish, A. Mizrahi, L. Schachter, C. Sears, G. R. Werner, and R. B. Yoder, "Dielectric laser accelerators," Reviews of Modern Physics **86**, 1337 (2014).
11. K. Wootton, J. McNeur, and K. Leedle, "Dielectric laser accelerators: designs, experiments, and applications," Reviews of Accelerator Science and Technology **9**, 105–126 (2016).
12. K. J. Leedle, A. Ceballos, H. Deng, O. Solgaard, R. F. Pease, R. L. Byer, and J. S. Harris, "Dielectric laser acceleration of sub-100 keV electrons with silicon dual-pillar grating structures," Optics Letters **40**, 4344–4347 (2015).
13. J. Breuer, J. McNeur, and P. Hommelhoff, "Dielectric laser acceleration of electrons in the vicinity of single and double grating structures–theory and simulations," Journal of Physics B: Atomic, Molecular and Optical Physics **47**, 234004 (2014).

#336300 https://doi.org/10.1364/OE.26.022801
Journal © 2018 Received 27 Jun 2018; revised 4 Aug 2018; accepted 6 Aug 2018; published 21 Aug 2018

Optics EXPRESS

14. M. Kozák, M. Förster, J. McNeur, N. Schönenberger, K. Leedle, H. Deng, J. Harris, R. Byer, and P. Hommelhoff, "Dielectric laser acceleration of sub-relativistic electrons by few-cycle laser pulses," Nuclear Instruments and Methods in Physics Research Section A: Accelerators, Spectrometers, Detectors and Associated Equipment **865**, 84–86 (2017).
15. M. Kozák, P. Beck, H. Deng, J. McNeur, N. Schönenberger, C. Gaida, F. Stutzki, M. Gebhardt, J. Limpert, A. Ruehl, I. Hartl, O. Solgaard, J. Harris, R. Byer, and P. Hommelhoff, "Acceleration of sub-relativistic electrons with an evanescent optical wave at a planar interface," Optics Express **25**, 19195–19204 (2017).
16. H. Deng, J. Jiang, Y. Miao, K. J. Leedle, H. Li, O. Solgaard, R. L. Byer, and J. S. Harris, "Design of racetrack ring resonator based dielectric laser accelerators," arXiv preprint arXiv:1701.08945 (2017).
17. J. McNeur, M. Kozák, N. Schönenberger, K. J. Leedle, H. Deng, A. Ceballos, H. Hoogland, A. Ruehl, I. Hartl, R. Holzwarth, O. Solgaard, J. S. Harris, R. L. Byer, and P. Hommelhoff, "Elements of a dielectric laser accelerator," Optica **5**, 687–690 (2018).
18. F. Lemery, K. Floettmann, P. Piot, F. Kärtner, and R. Aßmann, "Synchronous acceleration with tapered dielectric-lined waveguides," Physical Review Accelerators and Beams **21**, 051302 (2018).
19. A. Hanuka and L. Schächter, "Trapping of sub-relativistic particles in laser driven accelerators," Physics of Plasmas **24**, 123116 (2017).
20. T. W. Hughes, S. Tan, Z. Zhao, N. V. Sapra, K. J. Leedle, H. Deng, Y. Miao, D. S. Black, O. Solgaard, J. S. Harris, J. Vuckovic, R. L. Byer, and S. Fan, "On-chip laser-power delivery system for dielectric laser accelerators," Physical Review Applied **9**, 054017 (2018).
21. E. D. Palik, *Handbook of optical constants of solids*, vol. 3 (Academic, 1998).
22. W. Shin and S. Fan, "Choice of the perfectly matched layer boundary condition for frequency-domain Maxwell's equations solvers," Journal of Computational Physics **231**, 3406–3431 (2012).
23. J. Sun, E. Timurdogan, A. Yaacobi, E. S. Hosseini, and M. R. Watts, "Large-scale nanophotonic phased array," Nature **493**, 195–199 (2013).
24. V. R. Almeida, R. R. Panepucci, and M. Lipson, "Nanotaper for compact mode conversion," Optics Letters **28**, 1302–1304 (2003).
25. Q. Xu, V. R. Almeida, R. R. Panepucci, and M. Lipson, "Experimental demonstration of guiding and confining light in nanometer-size low-refractive-index material," Optics Letters **29**, 1626–1628 (2004).
26. D. J. Jones, S. A. Diddams, J. K. Ranka, A. Stentz, R. S. Windeler, J. L. Hall, and S. T. Cundiff, "Carrier-envelope phase control of femtosecond mode-locked lasers and direct optical frequency synthesis," Science **288**, 635–639 (2000).
27. J. J. Sakurai and S. F. Tuan, *Modern quantum mechanics* (Addison-Wesley Pub. Co., 1994), revised ed.
28. M. I. Stockman, "Nanofocusing of optical energy in tapered plasmonic waveguides," Physical Review Letters **93**, 137404 (2004).
29. P. M. Lapostolle and A. L. Septier, *Linear Accelerators* (North Holland Publishing Company, 1970).
30. H. O. Jeschke, M. E. Garcia, M. Lenzner, J. Bonse, J. Krüger, and W. Kautek, "Laser ablation thresholds of silicon for different pulse durations: theory and experiment," Applied Surface Science **197**, 839–844 (2002).
31. J. Chen, D. Tzou, and J. Beraun, "Numerical investigation of ultrashort laser damage in semiconductors," International Journal of Heat and Mass Transfer **48**, 501–509 (2005).
32. B. Stuart, M. Feit, A. Rubenchik, B. Shore, and M. Perry, "Laser-induced damage in dielectrics with nanosecond to subpicosecond pulses," Physical Review Letters **74**, 2248 (1995).
33. B. Naranjo, A. Valloni, S. Putterman, and J. Rosenzweig, "Stable charged-particle acceleration and focusing in a laser accelerator using spatial harmonics," Physical Review Letters **109**, 164803 (2012).
34. D. A. Swenson, "Alternating phase focused linacs," Part. Accel. **7**, 61–67 (1976).
35. B. M. Cowan, "Three-dimensional dielectric photonic crystal structures for laser-driven acceleration," Physical Review Special Topics-Accelerators and Beams **11**, 011301 (2008).
36. U. Niedermayer, T. Egenolf, O. Boine-Frankenheim, and P. Hommelhoff, "Alternating phase focusing for dielectric laser acceleration," arXiv preprint arXiv:1806.07287 (2018).
37. S. Van Der Geer, O. Luiten, M. De Loos, G. Pöplau, and U. Van Rienen, "3D space-charge model for GPT simulations of high brightness electron bunches," (2005), vol. 175 of *Institute of Physics Conference Series*, pp. 101–110.
38. K. L. Jensen, P. G. O'Shea, D. W. Feldman, and J. L. Shaw, "Emittance of a field emission electron source," Journal of Applied Physics **107**, 014903 (2010).
39. U. Niedermayer, T. Egenolf, and O. Boine-Frankenheim, "Beam dynamics analysis of dielectric laser acceleration using a fast 6d tracking scheme," Physical Review Accelerators and Beams **20**, 111302 (2017).
40. A. Hanuka and L. Schächter, "Operation regimes of a dielectric laser accelerator," Nuclear Instruments and Methods in Physics Research Section A: Accelerators, Spectrometers, Detectors and Associated Equipment **888**, 147–152 (2018).
41. A. Ody, P. Musumeci, J. Maxson, D. Cesar, R. England, and K. Wootton, "Flat electron beam sources for dla accelerators," Nuclear Instruments and Methods in Physics Research Section A: Accelerators, Spectrometers, Detectors and Associated Equipment **865**, 75–83 (2017).
42. S. K. Selvaraja, P. Jaenen, W. Bogaerts, D. Van Thourhout, P. Dumon, and R. Baets, "Fabrication of photonic wire and crystal circuits in silicon-on-insulator using 193-nm optical lithography," Journal of Lightwave Technology **27**, 4076–4083 (2009).
43. W. Hu, K. Sarveswaran, M. Lieberman, and G. H. Bernstein, "Sub-10 nm electron beam lithography using cold

Optics EXPRESS

development of poly (methylmethacrylate)," Journal of Vacuum Science & Technology B: Microelectronics and Nanometer Structures Processing, Measurement, and Phenomena **22**, 1711–1716 (2004).
44. T. Hughes, G. Veronis, K. P. Wootton, R. J. England, and S. Fan, "Method for computationally efficient design of dielectric laser accelerator structures," Optics Express **25**, 15414–15427 (2017).
45. E. A. Peralta, "Accelerator on a chip: design, fabrication, and demonstration of grating-based dielectric microstructures for laser-driven acceleration," Ph.D. thesis, Stanford University (2015).
46. R. Siemann, "Energy efficiency of laser driven, structure based accelerators," Physical Review Special Topics-Accelerators and Beams **7**, 061303 (2004).
47. K. Bane and G. Stupakov, "Using surface impedance for calculating wakefields in flat geometry," Physical Review Special Topics-Accelerators and Beams **18**, 034401 (2015).
48. Y. N. Na, R. Siemann, and R. Byer, "Energy efficiency of an intracavity coupled, laser-driven linear accelerator pumped by an external laser," Physical Review Special Topics-Accelerators and Beams **8**, 031301 (2005).

1. Introduction

The interaction between light and electrons has been studied for decades and has inspired many applications. Recent progress in nanophotonics and material science has provided new opportunities for studying and utilizing light-electron interactions in nano-scale structures, including both on-chip free-electron light sources [1–3] and dielectric laser accelerators (DLAs) [4–6]. Compared to conventional particle accelerators, which have long been a critical tool in fundamental physics studies and medical applications, DLAs have the further potential to be compact in size. DLAs utilize the near fields in the vicinity of laser-driven dielectric structures to generate acceleration [4–6]. Due to the high damage threshold of dielectric materials [7] and the availability of high power pulsed lasers in the near/mid-infrared spectrum [8], DLA has the potential to provide high acceleration gradients on the order of 1 GV/m [5, 9]. Furthermore, advanced nanofabrication techniques allow for single-chip integration of various components, including electron sources, optical coupling and control systems, sub-relativistic and relativistic DLA structures, and radiation generation structures, making DLA a promising technology for developing compact and inexpensive accelerators suitable for medical applications such as medical imaging and radiation therapy [10, 11].

Sub-relativistic acceleration is a crucial component in DLAs because the electrons generated by on-chip sources are generally sub-relativistic. To achieve sub-relativistic acceleration, most DLA demonstrations utilize a driving laser beam propagating perpendicular to the electron trajectory [6, 12–14]. However, there has been recent exploration for sub-relativistic acceleration schemes where the laser power flow propagates in the same direction as the electron beam [15, 16]. These co-propagation designs have the potential to increase the interaction length between electrons and the laser beam. Kozák *et al*. demonstrated the acceleration of sub-relativistic electrons near a flat interface under the total internal reflection condition [15] and Deng *et al*. proposed a DLA design based on the near field of ring resonators [16]. A major challenge of long-distance sub-relativistic acceleration is the dephasing, which arises when the velocities of the accelerated particles increase and become mismatched with the phase velocity of the accelerating field. Therefore, a sub-relativistic accelerator must provide a mechanism for changing the phase velocity of the accelerating field along the channel. Two previously proposed solutions include chirped grating structures [17] and multiple staged ring resonators [16]. However, the resonant nature of these designs causes the acceleration gradient to be sensitive to fabrication errors, making it difficult to predict the appropriate amount of chirp needed and the potential damage fluence.

In this paper, we propose a DLA structure for sub-relativistic electrons based on a tapered slot waveguide geometry. This structure supports a guided mode that has a longitudinal electric field in the vacuum slot and co-propagates with the electrons. The geometric parameters of the slot waveguide are changed gradually along the particle trajectory as the velocity of the accelerated particle increases, which makes it possible to match the phase velocity of the accelerating mode with the increasing velocity of the accelerated electrons. This tapering scheme can be valuable to

accelerator platforms other than the DLA, for instance, the cylindrical dielectric-lined waveguide accelerator [18, 19]. Moreover, the tapered slot waveguide DLA is non-resonant and, therefore, relatively tolerant to both fabrication errors and laser parameters. To obtain the continuously changing geometric parameters of the tapered slot waveguide necessary to retain the synchronicity condition, we introduce a design method based on the eikonal approximation of the electric field and the relativistic electron dynamics. For demonstration, we show that a large total acceleration energy of 10 keV can be achieved in 30 μm for sub-relativistic electrons with initial energy around 80 keV. Moreover, the tapered slot waveguide accelerator can be integrated with an on-chip power delivery network [20], which is critical for achieving a multi-stage integrated particle accelerator on a chip.

The paper is organized as follows: In section 2, we present the theory and design principles of a tapered slot waveguide DLA. We give a concrete design with typical experimental parameters and verify the design method in section 3. In section 4, we analyze the tolerance against experimental imperfections, followed by a discussion about the damage factor of slot waveguide accelerator in section 5. We conclude in section 6.

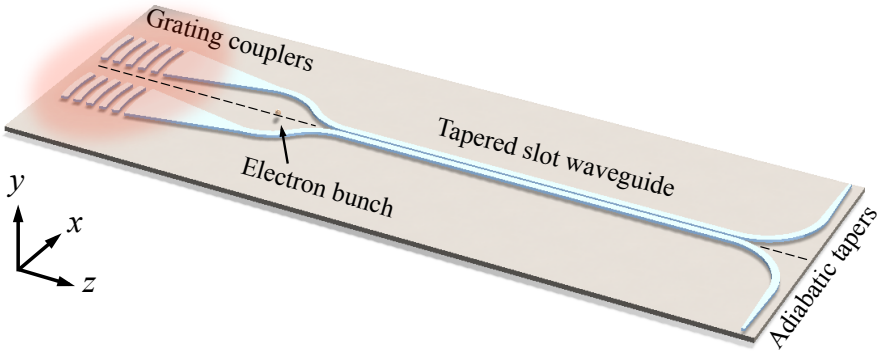

Fig. 1. A schematic of the tapered slot waveguide accelerator. Free space incident light is coupled into the guided wave through grating couplers. The two otherwise identical rectangular waveguides have different total lengths to accumulate a π phase difference. And they are bent and merged to form the slot waveguide. The slot waveguide width changes gradually in a certain distance before the two rectangular waveguides bend outwards and are adiabatically tapered to couple light out. The micro-bunched electron beam is propagating along the center of the slot, as indicated by the dashed line, in the same direction as the guided wave. Although the electrons may experience the electric field when traveling between two grating couplers, the net effect is negligible as the field and electron bunch are not synchronized.

2. Design principles

The proposed accelerator consists of a high-index slot waveguide sitting on a low-index substrate, as shown in Fig. 1. The slot waveguide consists of two identical rectangular waveguides separated by a sub-wavelength distance and is tapered along the propagation direction. The surrounding material is vacuum and the electron beam propagates through the central slot in the same direction as the guided mode. Light may be coupled into each rectangular waveguide through a grating coupler [23], and is transported into the slot waveguide through a bend in the waveguide. After certain acceleration distance, two rectangular waveguides bend outwards and light is coupled out through adiabatic tapers [24].

The slot waveguide, with certain geometric parameters, supports an acceleration mode that has

Optics EXPRESS

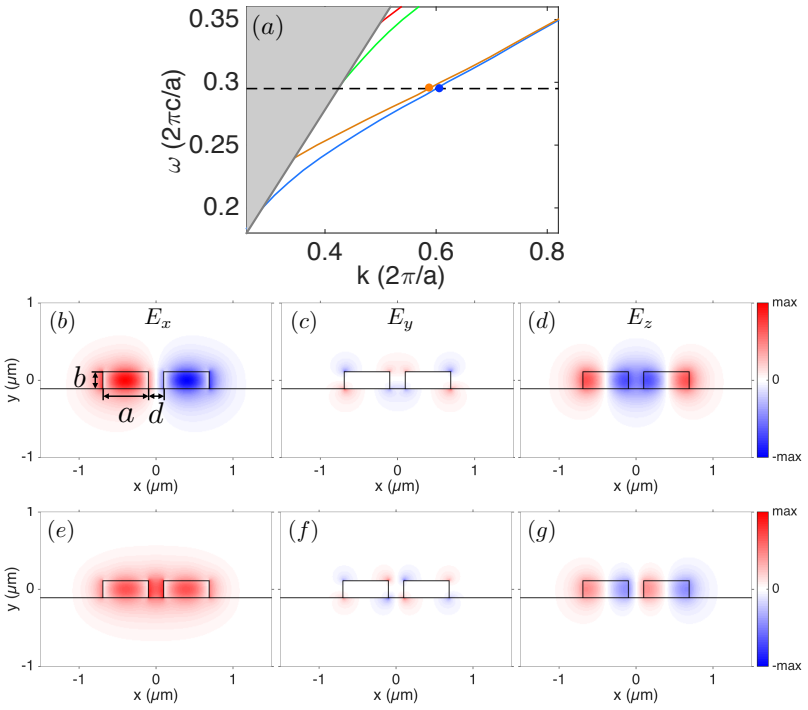

Fig. 2. Dispersion relation of a slot waveguide. (a) shows the dispersion relations of the guided modes supported by a slot waveguide made of silicon core on silica substrate with geometric parameters $a = 0.59$ μm, $b = 0.22$ μm, $d = 0.2$ μm, and refractive indices $n_{\mathrm{Si}} = 3.45$ and $n_{\mathrm{SiO_2}} = 1.44$ [21]. The blue and orange curve represent the fundamental and acceleration mode, respectively. The green and red curve represent higher order modes. The dashed line represents the chosen central frequency, $\omega = 2\pi c/2\mu$m. The gray region represents radiative modes. The transverse fields E_x, E_y and longitudinal field E_z are respectively shown in (b), (c), (d) for the acceleration mode, and in (e), (f), (g) for the fundamental mode. Each field component is plotted at a phase such that its amplitude is maximized. The phases of maximal amplitudes for the longitudinal and transverse fields differ by $\pi/2$. The dispersion relations and fields are solved using numerical eigenmode analysis [22].

a non-vanishing longitudinal electric field at the center of the slot [Fig. 2(d)]. These geometric parameters change gradually along the propagation direction such that the phase velocity of the acceleration mode always matches the velocity of the accelerated electron. The key dimensions of the slot waveguide are the width, a, and the thickness, b, of the rectangular waveguide and the width of the central slot, d. With standard lithographic nanofabrication techniques, tapering in the transverse direction can be achieved while continuous tapering in thickness is challenging. Also, the field strength decays as the distance from the high index core increases. Smaller d is favorable for larger acceleration gradient, though it requires electron beam with low transverse emittance in order to pass through the slot. With these considerations, we fix b and d, and change a along the propagation direction to tune the phase velocity of the acceleration mode.

To study the guided modes supported by the slot waveguide, we plot their dispersion relations in Fig. 2(a). The geometric dimensions are $a = 0.59$ μm, $b = 0.22$ μm, and $d = 0.2$ μm. The central wavelength of the pulsed laser is chosen to be $\lambda_0 = 2$ μm, which is below the silicon band gap energy to avoid absorption and allows for relatively large feature sizes and accessibility of high power pulsed lasers. Around the central frequency [indicated by the dashed line in Fig. 2(a)], the slot waveguide supports two guided modes. The fundamental mode has a strong transverse

Optics EXPRESS

electric field inside the slot [25] but zero longitudinal electric field at the center of the slot [Figs. 2(e)-2(g)]. The acceleration mode is the first excited mode containing a non-vanishing longitudinal electric field at the center of the slot, while the transverse electric field and the magnetic field have negligible magnitudes at the center of the slot due to the symmetry of the acceleration mode [Figs. 2(b)-2(d)]. This mode has an even symmetry with respect to $x = 0$ in contrast to the odd fundamental mode. By controlling the phase difference of light coupled into each of the rectangular waveguide, one can selectively excite the acceleration mode without the excitation of the fundamental mode. For instance, the two rectangular waveguides may have different lengths measured from the grating coupler to the slot waveguide to accumulate a π-phase difference between the guided waves in two rectangular waveguides before they merge into the slot waveguide, such that the acceleration mode can be excited under the illumination of a single laser beam with a beam spot covering the two grating couplers.

We proceed to investigate the condition that the tapered slot waveguide should satisfy such that the phase velocity and the velocity of the accelerated electron can be matched. Assume the tapered slot waveguide lies in z-direction from $z = 0$ to $z = L$. Since the acceleration mode has negligible transverse electric fields or magnetic fields at the center of the slot, we consider only the longitudinal field along the center of the slot in the following derivation. The longitudinal field at the beginning of the slot waveguide can be expressed as:

$$E_z(t, z = 0) = \eta\big(a(0)\big)\sqrt{P}A(t)\cos(\omega_0 t + \phi_0), \tag{1}$$

where η represents the longitudinal field per unit square root of power and is a function of a, i.e. $\eta = |E_z|/\sqrt{P}$, P is the peak power coupled to the acceleration mode, A is the temporal envelope of the electric field, ω_0 is the central frequency, and ϕ_0 is the carrier-envelope phase [26], which usually does not play a significant role in DLAs since the laser pulse duration is typically orders of magnitude longer than the optical cycle. For simplicity, we set $\phi_0 = 0$, and $t = 0$ when the profile of longitudinal field at $z = 0$ reaches the peak.

As the width of the slot waveguide changes continuously and gradually, the reflection and radiation loss are negligible. We also numerically find that both group velocity dispersion and self phase modulation effects are negligible for a waveguide with length on the order of tens of micrometers and a pulse duration on the order of hundreds of femtoseconds. Thus, the pulse profile and peak power remain approximately the same throughout propagation. Then, one can write the longitudinal electric field along the center of the tapered slot waveguide using the eikonal approximation which is also known as Wentzel-Kramers-Brillouin (WKB) approximation [27, 28].

$$E_z(t, z) = \eta\big(a(z)\big)\sqrt{P}A\Big(t - \int_0^z \frac{1}{v_g(z')}dz'\Big)\cos\Big(\omega_0 t - \int_0^z k(\omega_0; z')dz' + \phi_0\Big) \tag{2}$$

where $v_g(z)$ and $k(\omega; z)$ are respectively the group velocity and wave vector of the acceleration mode supported by the slot waveguide with the geometric parameters at z. The term related to the field envelope (A) takes into account the propagation of the pulse at a group velocity that gradually changes along the waveguide. The last term describes the phase of the electric field when the wave vector gradually changes as the wave propagates.

Suppose we have a specific tapered slot waveguide with phase velocity of the acceleration mode matching the velocity of a target electron, called a resonant particle [29], under a specified incident laser pulse. We denote the initial kinetic energy of the resonant particle as $E_{k,0}$, the time when the resonant particle enters the slot waveguide region as t_0, and assume that the resonant particle travels along the center of the slot waveguide. The time for the resonant particle to reach position z is

$$t(z) = t_0 + \int_0^z \frac{1}{v_e(z')}dz', \tag{3}$$

Optics EXPRESS

where $v_e(z)$ is the velocity of the electron at z. To obtain the acceleration field the resonant particle experiences, we substitute Eq. (3) into the field expression [Eq. (2)]. As the phase velocity of the acceleration mode matches the velocity of the resonant particle, i,e, $\omega_0/v_e(z) \equiv k(\omega_0; z)$, we notice that the phase of the electric field that the resonant particle experiences is fixed and can be reduced to

$$\phi_s = \omega_0 t_0 + \phi_0. \tag{4}$$

We refer to ϕ_s as the resonant phase. Moreover, since the envelope is a slowly varying function of space and time compared with the phase of electric field, we can substitute the electron velocity and group velocity in A using the values at the beginning of the slot waveguide. With these notations and approximations, the acceleration field felt by the resonant particle is

$$E_z(z) = \eta\big(a(z)\big)\sqrt{P}A\Big(t_0 + \frac{z}{v_e(0)} - \frac{z}{v_g(0)}\Big)\cos(\phi_s). \tag{5}$$

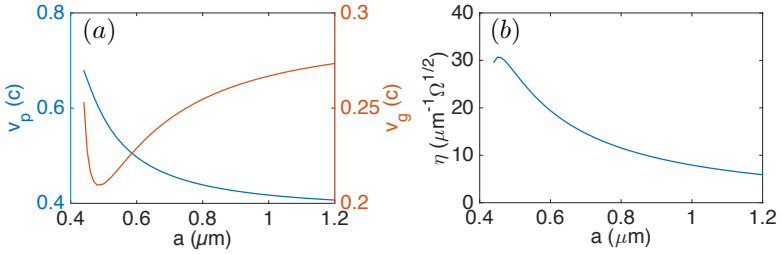

Fig. 3. Phase velocity, group velocity and power normalized longitudinal electric field as functions of width of the slot waveguide. The other parameters of the slot waveguide with silicon core and silica substrate are b = 0.22 μm, d = 0.2 μm, and working wavelength λ_0 = 2 μm. The phase velocity and group velocity of the acceleration mode supported by a uniform slot waveguide as a function of width are shown in (a), while the power normalized longitudinal electric field ($\eta = |E_z|/\sqrt{P}$) as a function of width is shown in (b) .

The dynamics of the resonant particle is governed by the relativistic Newton's Law.

$$-eE_z(z) = \frac{dE_k}{dz} = \frac{dE_k}{dv_e}\cdot\frac{dv_e}{da}\cdot\frac{da}{dz}, \tag{6}$$

where we denote the charge of the electron as $-e$, and the kinetic energy of the resonant particle as E_k. $E_k = mc^2(1/\sqrt{1-\beta^2} - 1)$, where $\beta = v_e/c$, and the velocity of the electron matches the phase velocity of the acceleration mode, i.e. $v_e(z) \equiv v_p(z)$. Combining the approximated expression of the longitudinal electric field and the relativistic Newton's law, one can obtain the differential equation that governs the tapering of the slot waveguide:

$$\frac{da}{dz} = \frac{-e}{mv_p(a)}\left(1 - \frac{v_p^2(a)}{c^2}\right)^{\frac{3}{2}}\left(\frac{dv_p(a)}{da}\right)^{-1}\eta(a)\sqrt{P}A\Big(t_0 + \frac{z}{v_e(0)} - \frac{z}{v_g(0)}\Big)\cos(\phi_s). \tag{7}$$

Equation (7) is the condition that the tapered slot waveguide should satisfy to match the phase velocity with the velocity of the accelerated electron. It provides the guidance to design the slot waveguide given the initial conditions of the electron, the temporal envelope and power of the excitation pulse, and the thickness and slot width of the slot waveguide. As both v_p and η are functions of a, the right hand side of Eq. (7) is a function of a and z. For instance, Fig. 3 shows $v_p(a)$, $v_g(a)$ and $\eta(a)$ for slot waveguides made of silicon core on silica substrate, with b = 0.22

Optics EXPRESS

μm and $d = 0.2$ μm, working at central wavelength $\lambda_0 = 2$ μm. Using the information in Fig. 3, we can get the width of the slot waveguide as a function of z by numerically solving Eq. (7).

In the following section, we give a concrete design of a tapered slot waveguide accelerator to demonstrate and verify our design principles.

3. Design for 80 keV electrons

To demonstrate the principles presented in Section 2, we design and analyze a 30 μm long tapered slot waveguide accelerator for electrons with initial kinetic energy of 80 keV under the illumination of a Gaussian pulse. Table 1 contains all the parameters we use in the design. We would like to further comment the following aspects of the selected parameters. (1) We choose silicon and silica as the core and substrate materials respectively, since the nanofabrication techniques are mature for this material system. Nevertheless, different core and substrate materials can be used, as long as the acceleration mode is phase velocity matched to the resonant particle. (2) Given that the acceleration gradient is limited by the damage threshold of dielectric materials, we limit the maximum electric field inside waveguide and substrate to be below 0.7 GV/m, which is below the electric field that corresponds to about half the damage fluence of silicon under the illumination of a 250 fs laser pulse at 2 μm wavelength [7, 30–32]. (3) The choice of a 30-μm acceleration length is a compromise between a high average acceleration gradient and a substantial energy gain, since the pulse peak of the acceleration field and the resonant particle may walk away due to different group velocities. (4) The resonant particle is accelerated when the resonant phase ϕ_s, as defined in Eq. (4), is between $\pi/2$ and $3\pi/2$, with maximum acceleration under $\phi_s = \pi$, since the acceleration force is proportional to $-e\cos(\phi_s)$ [Eq. (5)]. Longitudinal stability corresponds to resonant phase between 0 and π, such that leading electrons in an electron bunch experience a smaller acceleration and lagging electrons experience a larger acceleration. We choose the resonant phase to be $\frac{11}{12}\pi$, so the electron bunch remains stable in the longitudinal phase space. Therefore, reducing the resonant phase slightly away from π results in a preferable balance between large acceleration gradient and large longitudinally stable phase space. The transverse forces can be calculated using the Lorentz force equation with the electromagnetic fields of the acceleration mode of the slot waveguide, as shown in Figs. 2(b) - 2(d). Using the parameters shown in Fig. 2, we find that the transverse forces in x and y direction for the acceleration mode near the center of the slot waveguide are proportional to $ex\sin(\phi_s)$ and $-ey\sin(\phi_s)$ respectively, such that the focusing in x and y direction correspond to $\pi < \phi_s < 2\pi$ and $0 < \phi_s < \pi$ respectively. Transverse stability can possibly be achieved using ponderomotive focusing [33] or alternating phase focusing [34–36] with a low emittance electron beam, which is not discussed in detail within the scope of this study.

The design that matches the resonant particle given the parameters in Table 1 is shown in Fig. 4(a). The width of the slot waveguide is decreased from 0.59 μm to 0.554 μm in a 30 μm acceleration distance, which complies with the adiabatic condition [28]. As the width of the slot waveguide decreases, the phase velocity increases [dashed black curve in Fig. 4(b)]. The resonant particle, with 80 keV initial kinetic energy, is accelerated to 90 keV, which corresponds to an average acceleration gradient around 0.33 GV/m.

To validate the design principles presented in Section 2, the velocity of the resonant particle obtained by solving its dynamics is shown in the solid red curve in Fig. 4(b), in comparison with the phase velocity of the acceleration mode [dashed black curve in Fig. 4(b)]. The agreement suggests that the tapered slot waveguide designed using Eq. (7) satisfies the phase matching condition along the acceleration distance.

We also study the energy gain for electrons with initial conditions around the resonant particle, as shown in Fig. 4(c). We observe that the tapered slot waveguide is able to provide significant energy gain for electrons within a large range of initial conditions around the resonant particle. However, the large range of initial conditions for acceleration is mainly due to the

Optics EXPRESS

Table 1. Parameters in the design of a tapered slot waveguide accelerator for 80 keV electrons.

Parameter	Notation	Value	Unit
Slot waveguide length	L	30	μm
Slot waveguide thickness	b	0.22	μm
Slot waveguide slot width	d	0.2	μm
Slot waveguide width	a	0.554-0.59	μm
Slot waveguide core (silicon) refractive index	n_{core}	3.45	
Slot waveguide substrate (silica) refractive index	n_{sub}	1.44	
Initial energy of resonant particle	$E_{k,0}$	80	keV
Resonant particle entering time (measured from pulse peak)	t_0	123	fs
Resonant phase	ϕ_s	$11\pi/12$	rad
Central wavelength of incident pulse	λ_0	2	μm
Peak power in acceleration mode	P	320	W
Pulse duration (FWHM of intensity)	τ	250	fs
Maximum allowed electric field inside waveguide	E_{max}	0.7	GV/m

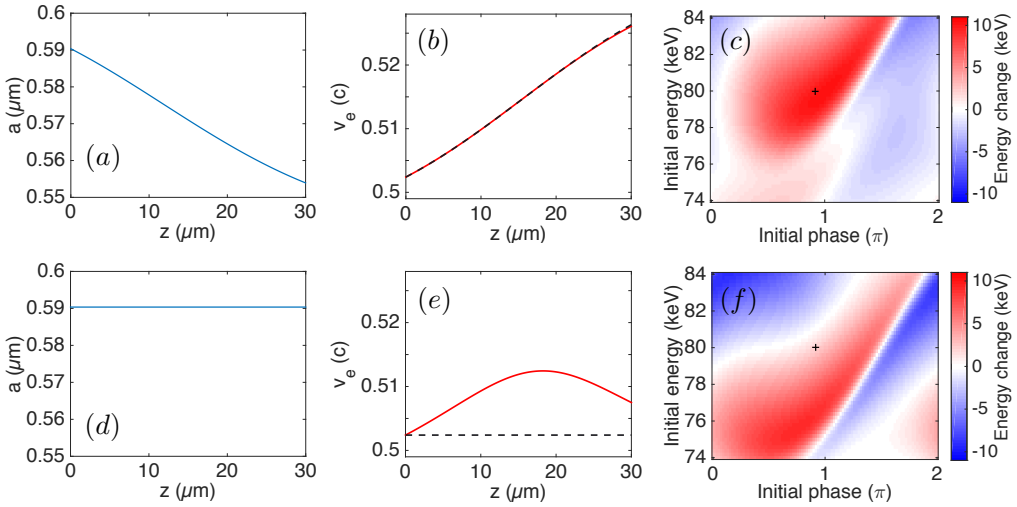

Fig. 4. Design of a tapered slot waveguide accelerator with parameters listed in Table 1. (a) shows the width of the slot waveguide which changes gradually along z direction. The velocity of the resonant particle along its trajectory is shown by the solid red curve in (b). The dashed black curve in (b) represents the phase velocity of the acceleration mode. The energy gain for electrons with different initial energies and different initial phases is shown in (c). The '+' indicates the initial conditions of the resonant particle. For comparison, the same analysis is conducted for a non-tapered slot waveguide, and the results are presented in (d)-(f).

short acceleration distance. With longer acceleration distance, the range of initial conditions for acceleration depends on the choice of the resonant phase and is likely to shrink. Also, we notice that the maximum negative energy change is less than the maximum positive energy change. This results from that the decelerated electrons, which are not always synchronized with the electric field, experience both acceleration and deceleration. In other words, continuous acceleration is achievable for electrons close to the resonant particle, while continuous deceleration is likely to be absent in our geometry.

Optics EXPRESS

To demonstrate the necessity of tapering, we study a non-tapered slot waveguide accelerator whose phase velocity matches 80 keV electrons [Fig. 4(d)]. The velocity of the electron with the same initial condition as the resonant particle for the tapered design is shown in Fig. 4(e). We find that the electron experiences acceleration at the beginning, but decelerate towards the latter half, due to the mismatch between the velocity of accelerated electrons and the phase velocity of the acceleration mode. Fig. 4(f) shows the energy gain for electrons with different initial conditions in a non-tapered slot waveguide. We observe that the electrons experiencing largest energy gain in a non-tapered slot waveguide have lower initial energy and smaller initial phase compared with the resonant particle in the tapered case. The dephasing of these electrons are relatively small since the average velocity of these electrons during acceleration is similar to the phase velocity of the acceleration mode and they almost always experience acceleration. However, these electrons cannot always experience peak acceleration force along the acceleration distance, since the velocity of the accelerated electron is not always the same as the phase velocity of the non-tapered slot waveguide. As a result, the maximum energy gain of a non-tapered slot waveguide is about 10% less than that of a tapered slot waveguide, as shown in Figs. 4(c) and 4(f). The relative difference between the maximum energy gain in the tapered case and the non-tapered case is going to further increase if the acceleration length increases.

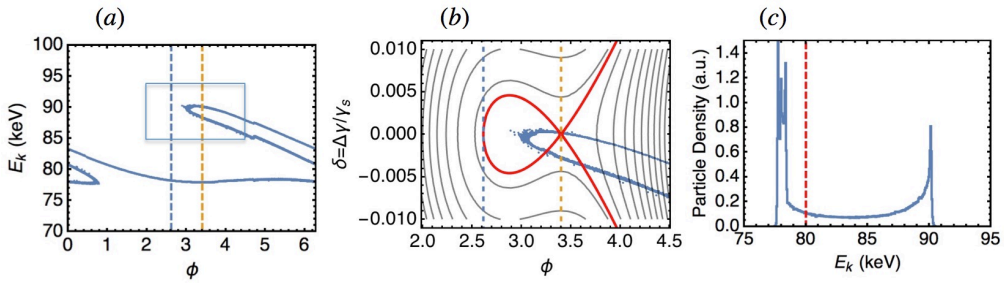

Fig. 5. Plots showing (a) the longitudinal distribution from particle tracking at the exit of the DLA; (b) overlay with the Hamiltonian phase space contours corresponding to the boxed region in part (a), showing that the highest energy electrons lie inside the Hamoltonian separatrix (red curve); (c) resulting energy distribution with a distinct peak of captured electrons at the target energy of 90 keV and the initial particle energy $E_{k,0}$ = 80 keV marked by the vertical dashed line.

To study the dynamics of the electrons traveling through this slot waveguide, we use the commercial code General Particle Tracer (GPT) [37] to track an injected distribution of electrons through the electromagnetic fields of the structure shown in Fig. 2. We consider two cases: (1) an initially unbunched uniform “cigar" beam of 50 fs duration and (2) a pre-bunched Gaussian beam of 100 as duration injected at the resonant phase ϕ_s. In both cases, an initial normalized beam emittance $\epsilon_{n,x} = \epsilon_{n,y} = 0.1$ nm is assumed, consistent with estimated emittances of nanotip emission sources [38], with a starting energy of 80 keV and an initial transverse RMS spot size of $\sigma_x = \sigma_y = 32$ nm in both transverse dimensions. Case (1) corresponds physically to the situation of many current experiments using low-current electron microscope sources [12], where there is effectively no space charge force between particles, because they are injected at random times and sample all phases of the electromagnetic field in the structure. Due to the microbunching effect of the fields, the final distribution in z is periodic with periodicity $\beta_s\lambda_0$, where $\beta_s = v_p/c$ is the local normalized phase velocity. We show in Fig. 5(a) the final particle distribution in longitudinal space (kinetic energy E_k vs. phase ϕ) over a single period. The results are analogous to solving the longitudinal equations of motion for an ensemble of particles using the standard formalism for the Hamiltonian longitudinal dynamics in a moving bucket

Optics EXPRESS

accelerator subject to the accelerating field of Eq. 2. To illustrate this, in Fig. 5(b) we superimpose the boxed region of the plot from part (a) with level sets of the corresponding Hamiltonian $H(\phi, \delta) = (\beta_s^2/2\gamma_s)\delta^2 + \alpha_0[1 - \sin\phi + (\phi - 3\pi/2)\cos\phi_s]$, where β_s and γ_s are respectively the velocity and Lorentz factor for the resonant particle, $\alpha_0 = eE_0\lambda_0/(2\pi mc^2)$, and $\delta = (\gamma - \gamma_s)/\gamma_s$ is the fractional energy deviation. The "captured" portion of the beam is seen to be contained within the separatrix shown in red in Fig. 5(b) which also corresponds to the peak at 90 keV in the final energy spectrum of Fig. 5(c). Since the DLA structure in this example is only 15 optical periods long in the z dimension, the particles undergo less than one synchrotron revolution in longitudinal phase space. If this process were extended over many stages of acceleration, the captured particles would continue to execute multiple synchrotron orbits within the accelerating "bucket" defined by this separatrix.

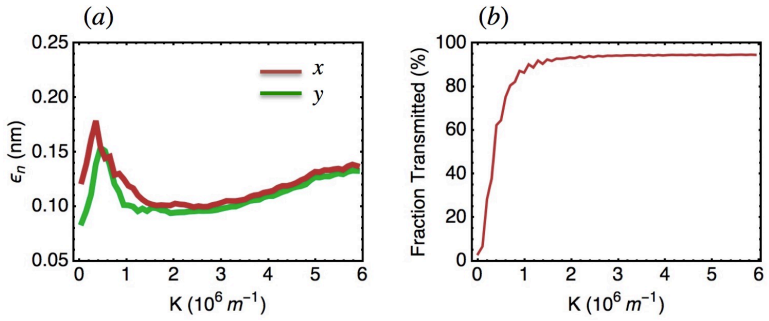

Fig. 6. Plots showing (a) normalized transverse emittance for a 100 attosecond bunched beam containing 470 electrons and (b) transmitted fraction as a function of external focusing field K.

For the second case, we study an electron beam that is pre-bunched such that it stays mainly in the longitudinally stable phase space region of Fig. 5(b). We assume the bunch consists of electrons with the same initial energy and within a duration of 0.1 fs and an initial normalized emittance $\epsilon_{n,x} = \epsilon_{n,y} = 0.1$ nm, as in Case (1). When the current is low, i.e. each micro bunch contains only a few electrons, we find that the transverse emittance growth is negligible. However, as the number of the electrons contained in each micro-bunch increases, the Coulomb space charge repulsion among the electrons can significantly contribute to the transverse emittance growth. Consequently, part of the electron beam may intercept the wall, and the number of electrons that pass through the slot waveguide decreases. To numerically simulate this effect, we extend the numerical field of the tapered slot waveguide design to 3D by applying the WKB approximation of Eq. 2 to vary the 2D transverse field map in phase velocity along the length of the accelerator. In the particle tracking simulation, a collimation filter is included to remove any particles that would travel outside the slot. We ignore the deflection of the beam due to image-charges, which is usually weak and commonly ignored in the study of dielectric laser accelerators [39]. To counteract the space-charge repulsion and confine the particles to the accelerating channel some form of focusing is needed. The estimated bunch charge for optimal acceleration efficiency in this structure is $q_{\text{opt}} = 75$ aC or approximately 470 electrons, which will be discussed in Section 5. In Fig. 6(a) we plot the normalized emittance of the beam in both transverse coordinates for a bunch of this charge and show the corresponding fraction of transmitted electrons in part (b) as a function of an applied external focusing field. The focusing force K may be interpreted as the linear focusing term appearing in a z-dependent paraxial ray equation of the form $x''(z) = -K^2 x(z)$. We note that the required focusing strength for optimal emittance preservation and near 100% transmission in Fig. 5 ($K \simeq 2 \times 10^6 \text{m}^{-1}$) is of the order of magnitude estimated in Section IV.A.4 of [10] as being required for focusing of

Optics EXPRESS

sub-relativistic electron beams in DLA structures. The apparent dip in emittance near $K = 0$ is due to the fact that with the focusing turned off so few electrons are transmitted that the emittance appears spuriously low. For the present tracking simulation we use a solenoidal magnetic field B oriented in the z direction, which provides a transverse focusing force $K = eB/2mc\beta_s\gamma_s$. The minimum emittance point of Fig. 6(a) corresponds to a field $B \simeq 4$ kT, which is impractically large. However, comparable K values can in principle be produced using electrostatic lenses or by compatible electromagnetic techniques such as alternating phase focusing or ponderomotive focusing using higher order space harmonics of the accelerating field [33]. Although a detailed analysis of compatible focusing methods is beyond the scope of this paper, some comparisons are provided in [36, 39–41].

4. Tolerance analysis

In this section, we study the tolerance of the tapered slot waveguide design given in Section 3 against experimental errors. We investigate how the energy gain of the resonant particle varies with respect to slightly perturbed parameters. Figure 7(a) shows the energy gain of the resonant particle when the peak power coupled into the acceleration mode deviates from the designed peak power. We find that the difference in energy change is less than 10% for power variance within 20%. The power level in actual experiments can be controlled with much higher accuracy. We also consider fabrication uncertainties where the width of the slot waveguide differs from the designed value. We analyze a typical scenario where the width of the slot waveguide changes by the same amount along the whole structure with all the other parameters fixed, i.e. $a(z) \rightarrow a(z) + \Delta a$. The energy gain of the resonant particle as a function of waveguide width deviation is shown in Fig. 7(b). The energy gain varies smoothly with fabrication deviation, and for waveguide width deviation up to 5 nm, the energy gain varies less than 20%. Although the fabrication error less than 5 nm is quite a tight experimental requirement, it is achievable using modern nanofabrication technologies [42, 43]. We further analyze how the shift of central frequency of the laser pulse influences the acceleration [Fig. 7(c)]. The variance of energy gain is negligible for a central wavelength shift within 10 nm. The robustness against central wavelength shift results from the non-resonant nature of the tapered slot waveguide. In Figs. 7(b) and 7(c), the peaks of the curves are shifted from zero deviation due to the resonant phase we choose. Through tolerance analysis, we find that the accuracy requirements of the slot waveguide accelerator design can be met by state-of-art nanofabrication and laser technologies.

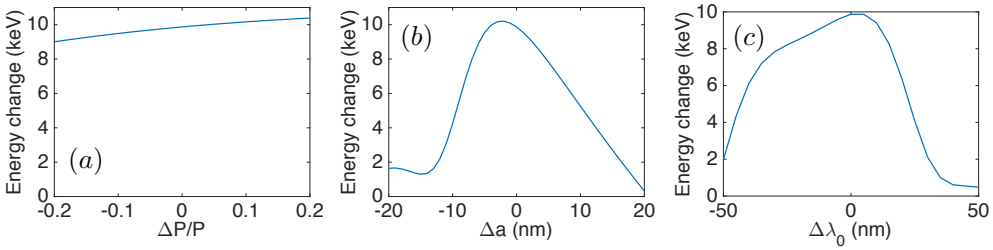

Fig. 7. Tolerance analysis. (a), (b) and (c) show the energy change of the resonant particle with variation in the input power, waveguide width, and central wavelength of laser pulse, respectively.

5. Discussion

In this section, we provide detailed information on how the “damage factor," an important figure of merit for dielectric accelerators, depends on the geometries of the slot waveguide. The damage

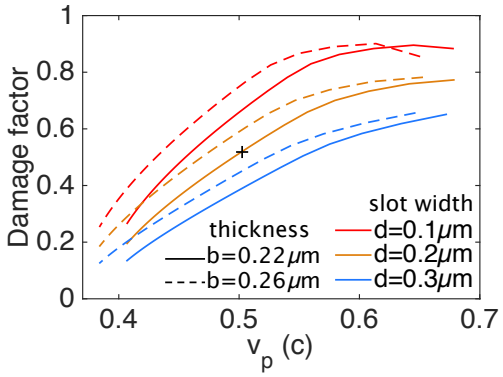

Fig. 8. Damage factor as a function of phase velocity for slot waveguides with different thicknesses or slot widths. v_p is the phase velocity of the accelerating mode. The solid and dashed curves respectively represent the damage factor for slot waveguides with thickness (b) 0.22 and 0.26 μm. The red, orange, and blue curves show the damage factor for slot waveguides with slot width (d) 0.1, 0.2 and 0.3 μm respectively. For each thickness and slot width, the waveguide width is changed to meet the phase velocity. The '+' represents the damage factor for parameters used in Fig. 2.

factor is the ratio of the maximum acceleration gradient at the center of the slot divided by the maximum electric field inside dielectric material, i.e. $|E_z|/E_{\max}$ [5]. As the acceleration gradient in DLA is limited by the damage threshold of the dielectric material, the damage factor functions as a figure of merit of the acceleration structure [44, 45]. For completeness, we numerically verify that the maximum electric field in the grating coupler is below the maximum electric field in the waveguides.

Figure 8 shows that the damage factor as a function of the phase velocity of the acceleration mode supported by the slot waveguide with different thicknesses and slot widths. We find that when the thickness increases, the damage factor increases at low phase velocity range, and lower phase velocity can be achievable. This happens because the phase velocity of the acceleration mode is lower bounded by the phase velocity of fundamental mode supported by the slab waveguide with same thickness and because a smaller phase velocity of the fundamental mode is associated with thicker slab. A similar trend is also found by Kozák *et al*. [15], which shows that a higher refractive index dielectric provides a larger damage factor and a lower minimal phase velocity in a DLA based on total internal reflection. Although a slot waveguide with a larger thickness may accelerate electrons with lower kinetic energy, a challenge is that a slot waveguide with large thickness and width usually supports more guided modes than the fundamental and acceleration mode. We find that the minimum electron velocity that a slot waveguide accelerator consisting of two single-mode rectangular silicon waveguides can synchronize with is around 0.45c ($E_k \approx 60$ keV). This value is obtained by numerically simulating silicon slot waveguides with a range of geometrical parameters, thus specific for silicon-on-insulator material system. The acceleration of electrons with lower velocity is also possible, up to c/n_{core}, using the tapered slot waveguide accelerator. However, more care should be taken to selectively excite only the acceleration mode.

Figure 8 also shows that the damage factor is smaller when the slot width becomes larger. This is because the near field intensity decays away from the interface of the high index dielectric. Also, the near field generally decays more slowly for acceleration modes with larger phase velocity [13]. Thus, the damage factor in general increases with the phase velocity of the acceleration mode (Fig. 8). The highest phase velocity of the acceleration mode supported by the slot waveguide is

Optics EXPRESS

limited by c/n_{sub}, where n_{sub} is the refractive index of the substrate underneath the high index waveguide. When the phase velocity of the mode is larger than c/n_{sub}, the mode becomes a radiative mode and leaks into the substrate. For our slot waveguide design, this phase velocity upper bound is 0.69c ($E_k \approx 195$ keV). Just before the acceleration mode becomes a radiative mode, the transverse size of the acceleration mode increases and the field profile deviates from the acceleration mode shown in Fig. 2(d). This results in the decrease of damage factor as phase velocity approaches the upper bound (Fig. 8). Nevertheless, this upper limitation can be overcome and the acceleration of electrons with velocity close to c can be achieved if the silica underneath the waveguide is removed.

The tapered slot waveguide accelerator can be cascaded to increase the acceleration distance and the energy gain. Within each stage, the width of the slot waveguide is continuously changed. Among different stages, the thickness and the slot width can also be changed, which gives more degrees of freedom to achieve synchronization conditions and to transport the electrons. The phases of the incident laser pulses coupled to different slot waveguide acceleration stages should be controlled. Besides free-space phase locking, the phase control may also be achieved through on-chip phase shifters if the laser power is delivered to the slot waveguide accelerators through a waveguide network [20]. The alternating phase focusing scheme may be applied to the cascaded tapered slot waveguide accelerator. By choosing different resonant phases (ϕ_s) in different stages, it is possible to achieve stable acceleration [34–36]. Nevertheless, the overall acceleration gradient is likely to decrease when the resonant phases are chosen further away from π.

Finally, we provide a heuristic estimation of the beam-loaded efficiency η_q of energy transfer from the electromagnetic mode of the structure to an electron bunch of charge q. We follow the prescription of Ref. [46] with some modification to account for the planar geometry of the slot waveguide structure. The loaded gradient for bunched beam operation can be written $G = G_0 - G_H$ where G_0 is the unloaded gradient and G_H is the Cherenkov retarding field. These are respectively given by $G_0 = (Z_C P/\lambda_0^2)^{1/2}$ and $G_H = qcZ_H/\lambda_0^2$, where Z_C and Z_H are the characteristic impedance and the Cherenkov wake impedance respectively and P is the power in the mode. The value $Z_C = 1.3$ kΩ is obtained directly from the field simulations of Fig. 2. A conservative estimate of Z_H for a narrow rectangular channel is given by [47] as $Z_H = \pi Z_0 \lambda_0^2/4d^2$, where d is the channel width and Z_0 is the impedance of free space, and the value for our design is $Z_H = 29.5$ kΩ. The resulting single-bunch efficiency $\eta_q = qcG\beta_g/[P(1-\beta_g)]$, where $\beta_g = v_g/c = 0.23$, is a quadratic function of q. Maximizing the efficiency gives an optimal bunch charge $q_{\mathrm{opt}} = 75$ aC, $\eta_{\mathrm{opt}} = 0.35\%$, which corresponds to a bunch charge of 470 electrons and a loaded gradient $G = G_0/2$. Consequently for proper operation with bunched beams, the structure's resonant phase velocity must be reoptimized to match the loaded gradient. An extended optimization of this structure geometry for high efficiency thus remains a task for future work. However we note that employing the multi-bunch efficiency formulas derived in [48], the corresponding efficiency for a bunch train of 37 bunches (which would fall within the RMS pulse duration of 250 fs assumed above), is 7.1% with no recycling of the laser power and is 27 % if the laser power is recycled within an on-chip laser cavity with a cavity loss of 2% and end-mirror reflectivity of 76%.

6. Conclusion

We have introduced a tapered slot waveguide DLA structure for sub-relativistic electron acceleration with continuous phase synchronization. With a semi-analytical expression of the field, we derive a differential equation describing the tapering necessary to achieve this condition. Using experimentally achievable parameters, we give an exemplary design for 80 keV electrons based on a silicon-on-insulator platform. It shows 10 keV of energy gain within 30 μm (0.33 GeV/m), which is a higher total acceleration energy than from DLA schemes with constant phase velocity [13, 15] and an acceleration gradient comparable to grating-based DLA structures [12]. We verify the robustness of such a design with respect to initial condition variations and experimental errors.

Optics EXPRESS

This geometry provides a promising avenue for the acceleration of sub-relativistic electrons and an effective method for providing an accelerating field that can maintain extended synchronicity with electrons of increasing velocities.

Funding

Gordon and Betty Moore Foundation (Accelerator on a Chip International Program - ACHIP, GBMF4744)

Acknowledgments

We wish to acknowledge our collaborators in the ACHIP collaboration. Special thanks to Dr. Martin Kozák, Yu Miao, and Dr. Yu Shi for suggestions and help.